Optics Letters

Self-mode-matching compact low-noise all-solid-state continuous wave single-frequency laser with output power of 140 W

Yixiao Wei,[1] Weina Peng,[1] Jiawei Li,[1] Pixian Jin,[1,2] Jing Su,[1,2] Huadong Lu,[1,2,*] and Kunchi Peng[1,2]

[1]State Key Laboratory of Quantum Optics and Quantum Optics Devices, Institute of Opto-Electronics, Shanxi University, Taiyuan 030006, China
[2]Collaborative Innovation Center of Extreme Optics, Shanxi University, Taiyuan 030006, China
*Corresponding author: luhuadong@sxu.edu.cn

Received 13 October 2022; revised 13 December 2022; accepted 14 December 2022; posted 19 December 2022; published 24 January 2023

The high power all-solid-state continuous wave single-frequency laser is a significant source for science and application due to good beam quality and low noise. However, the output power of the laser is usually restricted by the harmful thermal lens effect of the solid gain medium. To address this issue, we develop a self-mode-matching compact all-solid-state laser with a symmetrical ring resonator in which four end-pumped Nd:YVO_4 laser crystals are used for both laser gain media and mode-matching elements. With this ingenious design, the thermal lens effect of every laser crystal can be controlled and the dynamic of the designed laser including the stability range and the beam waist sizes at crystals can be manipulated only by adjusting the pump power used on each laser gain medium. Under an appropriate combination of pump powers on four crystals, self-mode-matching in a resonator is realized. A stable CW single-frequency at 1064 nm with 140-W power, 102-kHz linewidth, and low intensity noise is obtained. The presented design paves an effective way to further scale-up the output power of a compact laser by employing more pieces of gain media. © 2023 Optica Publishing Group

https://doi.org/10.1364/OL.478137

All-solid-state continuous wave (CW) high power single-frequency lasers with excellent beam quality, high power stability, narrow linewidth, and low noise have profound impacts in a variety of research and application fields including quantum optics and quantum information [1], atom physics [2], high-precision measurement [3], and so on. With the rapid development of science and technology, the requirement is needed to scale up the output power of an all-solid-state CW single-frequency laser and, at the same time, to maintain the high quality of its output light beam. So far, scaling up the output power of the single-frequency CW laser mainly is implemented by means of laser amplification technologies [4–7], and the laser noises are also synchronously amplified during the process. However, single-frequency CW lasers with both high output power and low noise are urgently needed in many applications including quantum optics and precision measurement. It is desirable to build a compact single-frequency laser of high power and low noise without an additional amplification system. As is well known, there are two ways to enhance the output power of a laser, that is, increasing the length of the laser gain medium and increasing its incident pump power. For a laser diode (LD) end-pumped laser, the usable length of a gain medium is limited by the Rayleigh length and the incident pump power is limited by the thermal lens effect of a laser crystal. The severe thermal lens effect will rapidly narrow the stability range of the laser, destroy the mode matching between the pump and laser modes which causes the fierce mode competition, and result in destructive crystal fracture under severe cases. For a single resonator laser with a bulk gain medium, the obtained highest output power was 50.3 W [8]. In 2018, our group developed a single-frequency CW 1064-nm laser with the output power of up to 101 W [9], which was implemented in a single ring resonator including two identical laser crystals. To achieve the precise mode self-reproduction of both gain crystals, a pair of lenses with identical focal length of 100 mm were placed inside the laser resonator. Due to the fixed focal lengths of the two lenses, the stability range of the designed laser was quite narrow and the laser only would be operated at a given incident pump power, thus the further improvement of the output power was restricted. Moreover, for realizing the higher power and stable single-longitudinal-mode operation in this laser, the optical length between the imaging lenses had to be precisely adjusted, which increased the difficulty of the laser debugging.

In this Letter, we present a high-power CW single-frequency 1064-nm laser with output power of up to 140 W, in which four pieces of Nd:YVO_4 crystals are placed in a single resonator to be the gain media and each laser crystal is independently pumped by an LD pump source. Usually, the thermal lens effect of the laser crystal is detrimental, which affects the stability and reduces the output power.. However, in the presented laser, we ingeniously make use of the thermal lenses of four crystals to comprise a set of the mode-matching lenses. Only by controlling the incident pump power on each crystal to change the focal lengths of their thermal lenses, the best mode-matching

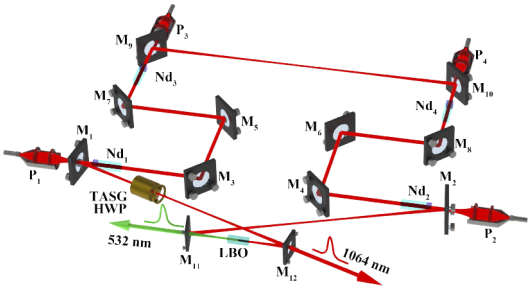


Fig. 1. Schematic diagram of designed self-mode-matching compact low-noise all-solid-state CW single-frequency 1064-nm laser. P_{1-4}, pump; Nd_{1-4}, YVO_4+Nd:YVO_4; TSAG, terbium scandium aluminum garnet; HWP, half-wave plate; LBO, lithium triborate.

condition can be achieved and thus extra optical elements inside the resonator are not needed, which prominently reduce the intracavity losses and adjusting difficulty. The presented self-mode-matching laser with four crystals not only increases the length of the gain medium and decreases the probability of the laser damage due to independently pump with lower pump power on each one, but also reduces the intracavity elements to the maximum extent.

The schematic diagram of the designed self-mode-matching low-noise all-solid-state CW single-frequency 1064-nm laser is shown in Fig. 1. The ring resonator is a symmetrical structure including four identical laser crystals. Each of the laser crystals is an α-cut composite YVO_4+Nd:YVO_4 rod with a size of 3×3×23 mm^3 consisting of an undoped end cap of 3 mm and a concentration of 0.8% Nd^{3+}-doped rod of 20 mm. A wedge angle of 1.5° is cut at the second end face of each crystal to suppress the σ-polarization oscillation and enhance the superiority of the π-polarization mode. Both end-faces of YVO_4+Nd:YVO_4 crystals are coated with anti-reflection (AR) films at both 1064 nm and 888 nm. To precisely control the temperatures of laser crystals, each of them is closely wrapped with an indium foil and enclosed by water-cooled copper blocks adhered with a thermoelectric cooler for heat dissipation and is independently end-pumped by a fiber-coupled laser diode (Coherent, M1F4S22-888.3-120C-IS9.15M4O3T3W4) with the center wavelength at 888 nm and the maximal output power of 120 W. The diameters and numerical apertures of the coupling fibers are 400 μm and 0.22, respectively. Every pump laser beam is collimated using an aspherical lens with a focal length of 30 mm and focused by a second aspherical lens with the focal length of 100 mm to an approximate pump spot of 1300-μm diameter for optimal mode-matching. Both input couplers M_1 and M_2 are concave–convex mirrors with curvature radii of R=1500 mm, which are coated with high-transmission (HT) films at 888 nm and high-reflection (HR) films at 1064 nm, respectively. Two identical M_9 and M_{10} flat mirrors are coated with HT films at 888 nm and HR films at 1064 nm, respectively. The M_{11} and M_{12} are two plano–concave mirrors with the same curvature radii of R = −100 mm. The M_{11} is coated with HR films at 1064 nm and HT films at 532 nm, and the M_{12} is coated with partially reflective films at 1064 nm (R = 45%) and HT films at 532 nm, respectively. The M_{11} and M_{12} are the output mirrors for the lasers at 532-nm and 1064-nm wavelengths, respectively. A type-I non-critically phase-matched lithium triborate (LBO) crystal with the dimension of 3×3×18 mm^3 is employed to introduce a nonlinear loss for effectively suppressing the non-lasing mode oscillation of

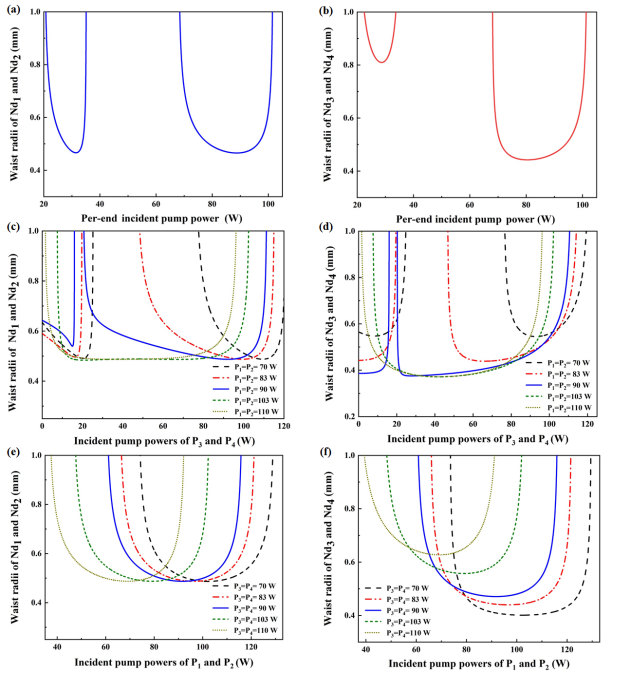


Fig. 2. Theoretical predictions of the mode size variations at the positions of the four laser crystals dependence on incident pump powers (P_1, P_2, P_3, P_4). (a) and (b) Incident pump powers of four laser crystals are synchronously increased. (c) and (d) Increasing the incident pump powers of P_3 and P_4 when P_1 and P_2 are fixed at 70 W, 83 W, 90 W, 103 W, and 110 W. (e) and (f) Increasing the incident pump powers of P_1 and P_2 when P_3 and P_4 are fixed at 70 W, 83 W, 90 W, 103 W, and 110 W.

the laser [10]. Both end faces of the LBO crystal are coated with AR films at both 1064 nm and 532 nm. It is placed at the beam waist between M_{11} and M_{12}, and its temperature is controlled to 148°C for phase matching by a home-made temperature controller with the precision of 0.01°C. Flat folding mirrors (M_3–M_8) with 45° incident angle and coated with HR films at 1064 nm are employed to reach an approximately 1.7-m optical cavity length. To eliminate the spatial hole burning effect and realize a stable unidirectional operation of the laser, an optical diode composed of a half-wave plate (HWP) and a 7-mm terbium scandium aluminum garnet (TSAG) crystal surrounded by a permanent magnet is placed in the resonator.

Figure 2 depicts the theoretical predictions of the mode size variations at the positions of the four laser crystals for the designed laser, where the abscissas have been converted to the incident pump powers (P_1, P_2, P_3, P_4) based on the dependence of the thermal lens focal length on the pump power given in Ref. [11]. Owing to the symmetric characteristic of the designed ring resonator, the cavity mode sizes at the centers of the Nd_1 and Nd_3 are equal to those of Nd_2 and Nd_4, respectively. Figures 2(a) and 2(b) show the dependence of the beam waist radii at the centers of Nd_1, Nd_2 and Nd_3, Nd_4 on the incident pump powers P_1, P_2 and P_3, P_4, respectively, when incident pump powers of four laser crystals are synchronously increased. It is shown that there are two stability ranges in the laser, which are from 20.5 W to 35 W and from 68.4 W to 101.4 W. It means that there is no laser to be generated when the four incident pump powers are simultaneously increased to the range between 35 W and 68.4 W without adjusting the cavity length. In this case, the incident

pump laser cannot be converted to the laser, and all pump energies are transferred to thermal energies in laser crystals which result in the rapidly elevating temperatures of the crystals. The laser will jump from the first stability range to the second one along with the increases of the pump powers. The calculated results show that the beam waist radii at the positions of the four laser crystals are equal 470 μm when the incident pump power on each of them is 90 W. In this case, the approximate focal lengths of the thermal lens effect in the four laser crystals used in the calculations are 210 mm. However, if we do not increase the incident pump powers of the four laser crystals synchronously, the new dynamic will emerge. Figures 2(c) and 2(d) illustrate the variation trends of the beam waist radii at the centers of Nd_1, Nd_2 and Nd_3, Nd_4 with the increases of P_3 and P_4 when P_1 and P_2 are fixed at 70 W, 83 W, 90 W, 103 W, and 110 W, respectively. These curves show that the stability ranges of the laser will move increasingly closer when P_1 and P_2 are increased. Moreover, the optimal waist radii at the centers of Nd_1 and Nd_2 for different P_1 and P_2 are basically the same. In contrast, the optimal waist radii at the centers of Nd_3 and Nd_4 will change rapidly with the variations of P_1 and P_2. Figures 2(e) and 2(f) show the dependence of the beam waist radii of four crystals on P_1 and P_2 when P_3 and P_4 are fixed at 70 W, 83 W, 90 W, 103 W, and 110 W, respectively. Different from Figs. 2(c) and 2(d), in this case, there is only one stability range. It can be attributed to the high P_1 and P_2 have provided sufficient thermal lens effect to ensure entering the stability range of the laser. Figure 2 shows that the dynamic of the designed laser including the stability range and the beam waist size of every laser crystal can be manipulated and the self-mode-matching is possible to be attained only by appropriately adjusting the incident pump power of each crystal.

To demonstrate the theoretical predictions in Fig. 2 and find the optimal self-mode-matching operation condition of the laser, the overall length and the distances between mirrors have to be slightly optimized repeatedly in the experiment. When the designed laser reaches the best condition, the dependencies of the 1064-nm laser output powers on the total incident pump powers of the four laser crystals are experimentally measured under four different dynamics. After the nonlinear LBO crystal is inserted into the resonator, a stable single-frequency CW 1064-nm laser with the maximum output power of 140 W is realized under the incident pump powers of P_1 = 86.2 W, P_2 = 83.5 W, P_3 = 106 W, and P_4 = 99.7 W (totally 375.4 W). The red stars curve in Fig. 3 depicts the output power as a function of total pump power on four laser crystals when they are synchronously increased. With the increase of the incident pump power, the output power increases first for the incident pump power larger than the threshold power of 68.8 W. However, when the incident pump power is greater than 150 W, the output power decreases with the increase of incident pump powers. At this moment, the temperature of every laser crystal rapidly increases because the incident pump laser is converted to heat. To prevent crystal damage due to the large temperature gradients, the incident pump power is rapidly increased artificially in the range from 150 W to 190 W. Once the incident pump power is beyond 190 W, the output power of the 1064-nm laser begins to increase once again. From the output power characteristic, double stability ranges (from 68.8 W to 150 W and 190 W to 375.4 W) for the designed laser are easily found, which is in good agreement with the previous theoretical prediction. To further investigate the dynamics of the built laser, we decrease the incident pump

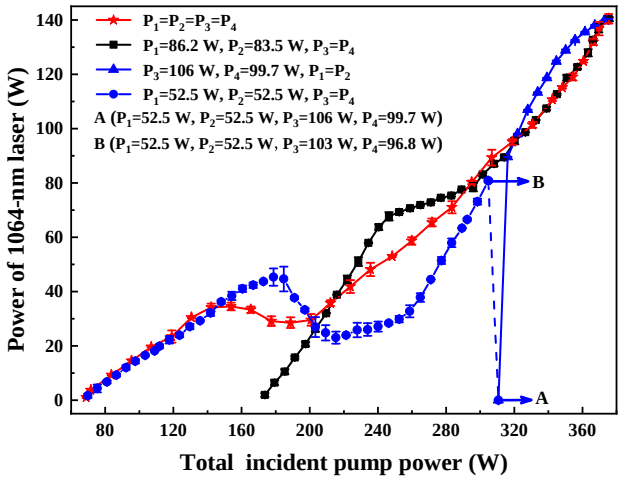


Fig. 3. Dependencies of 1064-nm laser output powers on the total incident pump powers of the four laser crystals under four different dynamics. The incident pump powers of four laser crystals are synchronously increased (red stars). Adjusting the incident pump powers of P_3 and P_4 while P_1 and P_2 are fixed on the maximal powers (P_1 = 86.2 W, P_2 = 83.5 W) (black squares). Adjusting the incident pump powers of P_1 and P_2 while P_3 and P_4 are fixed on the maximal powers (P_3 = 106 W, P_4 = 99.7 W) (blue triangles). Adjusting the incident pump powers of P_3 and P_4 while P_1 and P_2 are 52.5 W (blue dots).

powers of P_3 and P_4 while P_1 and P_2 are fixed at the maximal powers (P_1 = 86.2 W, P_2 = 83.5 W), and the recorded output power trend is shown in the black squares curve in Fig. 3. A bistability-like phenomenon is observed for the incident pump power in the range of 210 W to 290 W, which reveals that the thermal lens of the magneto-optical TSAG crystal can delay the output power decrease of the 1064-nm laser [12]. Likewise, when the incident pump powers P_1 and P_2 are decreased and P_3 and P_4 are still kept at the maximal powers, a bistability-like phenomenon is also observed, which is shown by the blue triangles curve of Fig. 3. However, the power region is different from that of the black squares curve in Fig. 3. The difference also reveals that the high incident pump powers of P_1 and P_2 can provide sufficient thermal lens effect to ensure the laser stays in the stability range.

The manipulation of the output characteristic for the built laser by adjusting the incident pump power can also be investigated from the blue triangles curve and the blues dots curve of Fig. 3. When the incident pump powers of P_1–P_4 are decreased to 52.5 W, 52.5 W, 106 W, and 99.7 W, respectively, the generated 1064-nm laser disappears (point A) because the laser has jumped out from the stability range. In this case, only by reducing the incident pump powers of P_3 and P_4 will the laser appears immediately (point B), which means that the built laser jumps into the stability range once again. When P_3 and P_4 continue to be reduced, a small pit similar to the red stars curve in Fig. 3 is observed, which further reveals the characteristic of the double stability range of the built laser.

From Fig. 3, we find the highest output power of 140 W is achieved when the incident powers of P_1–P_4 are 86.2 W, 83.5 W, 106 W, and 99.7 W, respectively. In this case, the peak-to-peak power fluctuation is recorded in Fig. 4(a), which is lower than ±1.1% in 5 hours. The observed power fluctuation with a probable period of 5 minutes is caused by the water-cooled

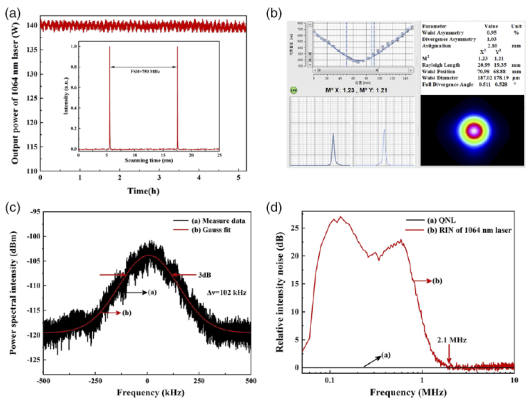


Fig. 4. Measured output performances of 1064-nm laser. (a) Power stability for 5 h and longitudinal-mode structure. (b) Transverse-mode characteristic. (c) Linewidth. (d) Relative intensity noise spectrum.

power meter. At the same time, the longitudinal-mode structure of the 1064-nm laser is monitored by employing a homemade Fabry–Perot cavity with a free spectral range of 750 MHz [13], and the monitored result is depicted in the inset of Fig. 4(a), which clearly shows that the stable single-longitudinal-mode operation is achieved. In particular, it is found that there is a wide range of the stable single-longitudinal-mode operation for a wide range around the maximal output power of 140 W, which is benefited from the sufficient nonlinear loss of nonlaser modes introduced by the nonlinear LBO crystal and the realization of self-mode-matching in the resonator. The transverse-mode characteristic of the obtained 1064-nm laser is measured by an M^2 beam quality analyzer (M2SETVIS, Thorlabs). The caustic curve and corresponding spatial beam profile are depicted in Fig. 4(b). The measured beam quality factors are $M_x^2 = 1.23$ and $M_y^2 = 1.21$, respectively. From these experimental results, we can know that the optimal self-mode-matching of the laser is achieved, and the theoretical predictions are in basic agreement with experimental results. The optimal mode-matching condition of the laser is realized under the incident pump powers of $P_1 = 86.2$ W, $P_2 = 83.5$ W, $P_3 = 106$ W, and $P_4 = 99.7$ W, which is slightly different from the theoretical predictions of 90 W for the four pump powers. It can be attributed to the inevitable errors of the experimental system including imperfect symmetry of the ring resonator and different absorption of each laser crystal.

The linewidth of the achieved laser is also measured by a delayed self-heterodyne interferometer and the result is shown in Fig. 4(c). It is seen that the measured linewidth of the single-frequency 1064-nm laser is as narrow as 102 kHz, which is attributed to the 1.7-m total cavity length of the built laser.

Lastly, the relative intensity noise (RIN) of the laser relative to the quantum noise limit (QNL) is measured by a homemade low-noise balanced homodyne detector and analyzed by a spectrum analyzer, which is recorded in Fig. 4(d). The black line represents the QNL and the red line represents RIN of the single-frequency 1064-nm laser. The frequency that the laser reaches QNL and the frequency and amplitude of the resonant relaxation oscillation (RRO) peak above the QNL are 2.1 MHz, 593 kHz, and 22.8 dB/Hz, respectively. It should be mentioned that the measured noise spectra below 0.2 MHz cannot represent the real intensity noise of the built laser, it is mixed with the electronic noises from the detector and the spectrum analyzer.

In conclusion, we present a self-mode-matching low-noise CW single-frequency 1064-nm laser with the output power of 140 W and linewidth of 102 kHz, which is realized by employing four Nd:YVO_4 laser crystals and each laser crystal is independently pumped by an LD pump source in a single resonator. Four laser crystals act as the gain media as well as the mode-matching elements, thus the usually used intracavity mode-matching lenses are not needed. Additionally, although the total incident pump power is high, it has been distributed among the four laser crystals, which well reduces the thermal effect and damage probability of every laser crystal. Moreover, the dynamics of the designed laser can be easily manipulated and a good mode-matching can be attained only by adjusting the incident pump powers of the four laser crystals. From the measured long-term power stability, beam quality factor, and intensity noise characteristic, we believe that the achieved high-power single-frequency CW 1064-nm laser is a good light source. On this basis, we will further reduce the intensity noise of the laser in the later work to satisfy the requirements of quantum information, gravitational-wave detection, and so on. Even more importantly, the method presented in this Letter paves a general way to scale up the output power of a CW single-frequency laser in a single resonator by employing more gain crystals.

Funding. National Natural Science Foundation of China (61975100, 62027821, 62105192); Applied Basic Research Program of Shanxi Province (20210302121004); Key Research and Development Program of Shanxi Province (202102150101002); Program for the Innovative Talents of High Education Institutions of Shanxi; Fund for Shanxi "1331 Project" Key Subjects Construction; Research Project Supported by Shanxi Scholarship Council of China (2022-015).

Disclosures. The authors declare no conflicts of interest.

Data availability. Data underlying the results presented in this Letter are not publicly available at this time but may be obtained from the authors upon reasonable request.

REFERENCES

1. S. Wehner, D. Elkouss, and R. Hanson, Science **362**, 303 (2018).
2. M. Endres, H. Bernien, A. Keesling, H. Levine, E. R. Anschuetz, A. Krajenbrink, C. Senko, V. Vuletic, M. Greiner, and M. D. Lukin, Science **354**, 1024 (2016).
3. L. Winkelmann, *Injection-locked high power oscillator for advanced gravitational wave observatories* (Cuvillier Verlag Göttingen, 2012).
4. C. Robin, I. Dajani, and B. Pulford, Opt. Lett. **39**, 666 (2014).
5. X. Zhang, J. Ye, X. Luo, X. Chen, L. Zhang, X. Xu, H. Ren, Y. Lu, Y. Ma, Q. Gao, J. Sun, and W. Wang, Opt. Express **29**, 5687 (2021).
6. F. Saltarelli, A. Diebold, I. J. Graumann, C. R. Phillips, and U. Keller, Optica **5**, 1603 (2018).
7. N. Bode, F. Meylahn, and B. Willke, Opt. Express **28**, 29469 (2020).
8. Y. Guo, H. Lu, M. Xu, J. Su, and K. Peng, Opt. Express **26**, 21108 (2018).
9. Y. Guo, M. Xu, W. Peng, J. Su, H. Lu, and K. Peng, Opt. Lett. **43**, 6017 (2018).
10. H. Lu, J. Su, Y. Zheng, and K. Peng, Opt. Lett. **39**, 1117 (2014).
11. M. E. Innocenzi, H. T. Yura, C. L. Fincher, and R. A. Fields, Appl. Phys. Lett. **56**, 1831 (1990).
12. Q. Yin, H. Lu, J. Su, and K. Peng, Opt. Lett. **41**, 2033 (2016).
13. Z. Shi, Y. Guo, M. Xu, and H. Lu, Journal of Quantum Optics **24**, 237 (2018).